River Flow 2010 - Dittrich, Koll, Aberle & Geisenhainer (eds) - © 2010 Bundesanstalt für Wasserbau ISBN 978-3-939230-00-7

The flow structure in the tail of a lock-exchange gravity current with a large volume of release propagating over dunes

T. Tokyay & G. Constantinescu
Civil and Environmental Engineering Department, The University of Iowa, Iowa City, Iowa, USA

ABSTRACT: The present study uses highly resolved Large Eddy Simulation (LES) to study the structure of the flow in the tail of a lock-exchange gravity current with a large volume of release for which the current propagates with a relatively constant front velocity over a large amount of time (slumping phase). The cases of a current propagating over large scale roughness elements in the form of an array of two-dimensional dunes or square ribs are considered. In the tail region situated far from the front, the flow eventually reaches a quasi-steady state. At this point the flow in this region becomes periodic in the streamwise direction. Thus, similar to the case of constant density channel flow over an array of identical roughness elements, to study the flow and turbulence structure in the quasi-steady region, it is sufficient to focus on the flow in between two consecutive roughness elements. The paper discusses the changes in the flow structure within the quasi-steady region function of the shape of the roughness elements (dunes vs. ribs) and with respect to the case of a current propagating over a smooth flat surface.

Keywords: Numerical Simulations, Gravity currents, Coherent Structures, Dunes

1 INTRODUCTION

Gravity currents (GCs) occur widely in nature. For example, erosion by gravity currents is one of the main causes for formation of submarine canyons on continental slopes and plays a determinant role in transporting sediments from shallower to deeper regions in water environments (e.g., rivers, reservoirs). Moreover, the loose bed surface over which gravity currents propagate in natural environments is often not smooth or flat. Bed forms, typically in the form of ripples, dunes or anti-dunes are present at the river bed. The presence of bed forms and topographic bumps, or of a vegetation layer, leads to an additional net drag force which slows down the gravity current (Hatcher et al., 2000, Tanino et al., 2005). The presence of large-scale bedforms provides an additional mechanism for energy dissipation and can substantially modify the capacity of a compositional gravity current to entrain sediment with respect to the case of a flat bed. Unfortunately, not much is known on the interaction of gravity currents with the bed morphology.

Studying gravity currents in the field is very difficult. Often, these currents develop in remote and hostile environments (e.g., in the deep part of large rivers and lakes). GCs on the bottom of large rivers occur infrequently and monitoring equipments are hard to install and to protect from the impact with the current. Thus, most of the information on the structure and evolution of GCs comes from laboratory experiments conducted at much smaller Reynolds numbers. Moreover, detailed measurements of the velocity and density fields within the gravity current at different stages of its evolution are seldom available even from experimental studies. Even less information is available from experiments on the changes in the flow and structure of the gravity current as it propagates over bedforms or as it interacts with underwater obstacles (e.g., submerged dams).

High-resolution eddy-resolving three-dimensional (3D) numerical simulations of GCs have the advantage that can provide this detailed information. For example, simulations of GCs propagating over a flat bed have been undertaken using Direct Numerical Simulation –DNS - (e.g., see Hartel et al., 2000, Cantero et al., 2006) and Large Eddy Simulation – LES - (e.g., Ooi et al., 2009). The propagation of intrusive gravity currents was investigated using LES by Ooi et al.

(2007a). Compared to DNS, LES allows performing simulations at Reynolds numbers that are closer to the range typically encountered in practical applications (Ooi et al., 2007b, 2009). Recently, LES was used to study the detail of the interaction between a gravity current and an isolated obstacle (bottom mounted square cylinder, circular cylinder situated close to the bed) and to estimate the unsteady forces and moments acting on the obstacles (Gonzales-Juez et al., 2009a, 2009b, 2010). This information is critical to the design of oil pipes and other underwater structures against possible hazard induced by the passage of a GC. The propagation of a GC over deformed boundaries or bedforms has received much less attention despite its importance for practical applications in river and coastal engineering. For example, Huang et al. (2005) performed a RANS study of a turbidity current propagating over a moving boundary driven by sediment entrainment and deposition at the bed. Even experimentally, there is very little work done for GCs propagating over bedforms. The related problem of a current propagating in a porous medium (e.g., vegetation layer) received more attention. This type of flows was studied experimentally and theoretically by Hatcher et al. (2000). There are important similarities and differences with the type of flows investigated in the present study. In both cases the changes with respect to a GC propagating over a flat surface occur due to the additional drag induced by the obstacles. However, while in the case of bedforms the added drag acts only over the lower part of the current, in the case of a current propagating through a porous medium the drag acts generally over all the height of the current. The degree to which some of the theory developed for GCs propagating through a porous medium applies for GCs propagating over bedforms is still unknown.

In the set up considered in this study, the GC containing lock fluid propagates in a rectangular horizontal plane channel (Fig. 1). We consider the case in which the initial volume of the release (heavier lock fluid) is high (x_0>>H) and occupies the whole depth of the channel (full-release case, h=H). The channel is long enough to avoid interactions of the GC with the end walls during the simulation time. Of particular interest for the present study is the structure of the tail of the GC. This is because in the case of GCs with a large volume of release propagating over bedforms most of the sediment is entrained beneath the tail of the current rather than the head and dissipative wake regions, as is the case for a current propagating over a flat bed (Ooi et al., 2009). The effect of the shape of the obstacles is studied based on differences observed in simulations conducted with an array of 2D dunes and ribs of equal height.

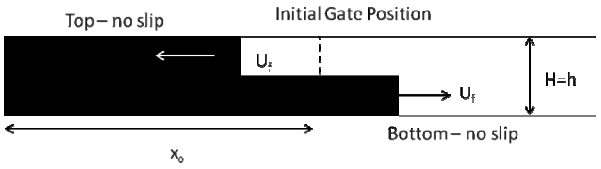

Figure 1. Sketch of the flow during the slumping phase for the case of a full depth release lock-exchange flow. The gate is positioned far from the extremities of the channel (x_0/H>>1). The evolution of the forward and backward propagating Boussinesq gravity currents is anti-symmetric.

2 NUMERICAL METHOD AND DESCRIPTION OF THE SIMULATIONS

A finite-volume LES code is used to solve the governing equations on non-uniform Cartesian meshes. A semi-implicit iterative method that employs a staggered conservative space-time discretization is used to advance the equations in time while ensuring second order accuracy in both space and time. A Poisson equation is solved for the pressure using multigrid. The algorithm discretely conserves energy, which allows obtaining solutions at high Reynolds numbers without artificial damping. A dynamic Smagorinsky model is used to estimate the subgrid-scale viscosity and diffusivity. All operators are discretized using central discretizations, except the convective term in the advection-diffusion equation solved for the concentration for which the QUICK scheme is used. Though no experimental data were available to validate the simulations of GCs propagating over a series of ribs and dunes, detailed validation of the code for 3-D LES simulations of cavity flows with or without an incoming turbulent flow is described in Chang et al. (2006). The same code was successfully used by Chang et al. (2007) to predict ejection of buoyant pollutants from bottom channel cavities and by Ooi et al. (2007a, 2007b, 2009) to predict the evolution of intrusive and bottom propagating currents at Reynolds numbers as high as $Re=10^6$, which is outside the range in which most laboratory experiments are conducted.

The density difference $\Delta\rho$ between the lock fluid and the ambient fluid is small enough to use the Boussinesq approximation. The Navier-Stokes equations and the advection-diffusion equation for the concentration are made dimensionless using the lock-gate opening, *h*, and the buoyancy velocity, $u_b = \sqrt{g'h}$, where $g'=g\Delta\rho/\rho_0$ is the reduced gravity and g is the gravity. The time scale is $t_0=h/u_b$. The non-dimensional concentration

is $C=(\overline{C}-\overline{C}_{\min})/(\overline{C}_{\max}-\overline{C}_{\min})$ where $\overline{C}_{\max}$, $\overline{C}_{\min}$ represent the maximum (lock fluid) and minimum (ambient fluid) concentrations in the domain and $\overline{C}$ is the dimensional concentration. The lock gate is positioned in the middle of the computational domain (x/H=0.0). The Reynolds number in all the simulations is Re=48,000.

Two types of obstacles are considered (Fig. 2). The 2-D dunes are representative of bedforms present at the bottom of rivers. The shape of the dunes is taken from the experiment of Mierlo and de Ruiter (1988). The ratio between the height, D, and the wavelength, λ, of the dune is 0.05, which is within the typical range observed for dunes in small and medium-size rivers. The dunes and ribs are of equal height (D=0.15H) and equal wavelength (λ=3H, λ/D=20). The top and bottom surfaces are simulated as no-slip smooth (flat or deformed) solid surfaces. A zero normal gradient boundary condition is assumed for the concentration at the top, bottom and at the two end boundaries. The viscous Schmidt number is taken equal to 600 corresponding to saline water. The flow field was initialized with the fluid at rest.

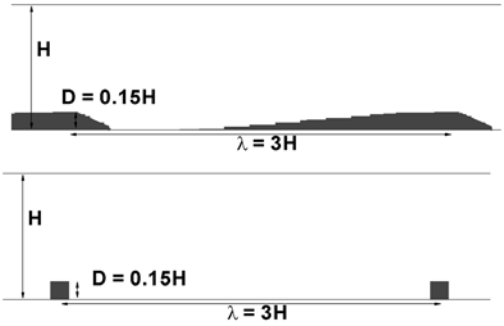

Figure 2. Sketch showing relative dimensions of the 2-D ribs and dunes used in the simulations

The presence of a flat bed, 2-D dunes or 2-D ribs is indicated by the presence of an F, D or R in the name used for the simulation. The non-dimensional height of the dunes or ribs, D/H*100 is indicated by a number. For example, LR-D15 refers to the simulation with 2-D dunes of height 0.15H conducted at Re=47,800.

The 3D mesh contained over 40 million cells (64 points in the spanwise direction). The mesh spacing in the wall normal direction was sufficiently small to resolve the viscous sublayer in the simulations. The time step was $0.001t_0$. A full simulation required one month on 48 processors of a XEON PC cluster.

To maintain the anti-symmetry of the forward and backward propagating currents containing lock and ambient fluid, respectively, in the simulations containing 2D dunes and ribs, the roughness elements were placed on the bottom surface in the region with x/H>0 and on the top surface in the region with x/H<0. This allows analyzing only the evolution of the forward propagating current containing heavier lock fluid.

3 FRONT VELOCITY

As expected, in the flat bed simulation (LR-F) the GC reaches a constant front velocity (slumping phase) a short time after the release of the lock gate. The predicted non-dimensional front velocity expressed as a Froude number ($Fr_f=U_f/u_b$) is 0.45, which is in very good agreement with experimental data. The front velocity remains constant until the end of the simulation.

The presence of ribs or dunes slows down the advancement of the front of the current compared to the flat-bed case after the first obstacle is reached at around $t=10t_0$. Still, in the simulations with small obstacles (D=0.15H) the mean slope of the trajectory followed by the front can be considered, in a good approximation, constant for $t/t_0>16$, after the front passed the first obstacle. This means that a slumping phase in which the front velocity is approximately constant is also present for GCs propagating over a surface containing a series of identical 2-D obstacles, at least for obstacles whose height is less than half that of the incoming current (case considered in present study).

The mean front velocity, U_f/u_b, is 0.4 and 0.34 in the LR-D15 and LR-R15 simulations, respectively. The mean value obtained from the front trajectory is in very good agreement with estimations of the mean front velocity based on the time it takes the current to advance between the crests of two successive dunes or between the upstream faces of two successive ribs. This mean that a slumping phase is present in the simulations with obstacles and the front velocity in the LR-D15 and LR-R15 simulations is 12% and, respectively, 24% lower than the value ($U_f/u_b=0.45$) predicted for the flat bed case. The difference is explained by the fact that ribs induce higher form drag due to their larger degree of bluntness.

Moreover, simulation results show that the flux of heavier fluid at streamwise sections situated in the region corresponding to a certain obstacle reaches a constant value when the front is situated sufficiently far from the obstacle. This happens a short time after the backward propagating hydraulic jump originating at the crest of the obstacle situated downstream of the one that is monitored, has propagated over the obstacle that is monitored. From that point on, the flow over that obstacle, or over the streamwise region associated with it in the case of ribs, can be considered to be quasi-steady. This is similar to the widely studied case of a constant density channel flow past an ar-

ray of ribs or dunes. Thus, the mean flow and turbulence structure in this region can be analyzed in a similar way.

4 TAIL STRUCTURE

The structure of the tail in the low Reynolds number simulations with a flat bed and with small obstacles at the bed is compared in Fig. 3 at times when the front is situated at x~18.5H.

Consistent with the findings of Ooi et al. (2009), the concentration distribution in Fig. 3a shows that in the flat bed case a stably stratified interface, depleted of large-scale eddies, develops between the heavier current and the lighter fluid, starting at the position of the lock gate. The stably stratified interface is slightly tilted toward the front region. The height of the high-density layer of fluid reaches a minimum at the end of the interface. It remains fairly constant in the dissipative wake region before increasing again in the head region. As a result of the presence of the tilted interface, the streamwise velocity inside the current peaks at the end of the tilted interface and over the upstream part of the dissipative wake region ($u\sim0.7u_b$). The velocity decreases gradually as the front ($U_f\sim0.45u_b$) is approached. The velocity magnitude is close to zero within the tilted interface layer containing mixed fluid (Fig. 3d).

The structure of the current is very different in the case dunes or ribs are present at the bed. A layer of varying height containing mixed fluid develops between the regions containing heavier fluid and ambient fluid. At large distances from the front, the top of this layer is close to horizontal in the simulations with obstacles at the bed. The bottom of this layer undergoes quasi-regular deformations with the same wavelength at that of the obstacles (λ=3H). The velocity magnitude inside this layer is very small (Fig. 3d). The reason for the formation of this layer is related to the formation of the jet-like flow past the crest of the obstacle and of the upstream propagating hydraulic jump as the front overtakes the obstacle. The extent of the jet-like flow corresponds to the regions of high velocity in Figs. 3c and 3d. The formation of the jet-like flow containing mostly higher-density fluid induces a strong shear layer on its outer side (toward the ambient fluid). Once they form, the jet-like flow and the associated shear layer are permanent features of the flow around the obstacle (Fig. 3b). The downstream extent of the shear layer past the crest or downstream face of the obstacle is larger in the case ribs are present (2.25H vs. 1.5H).

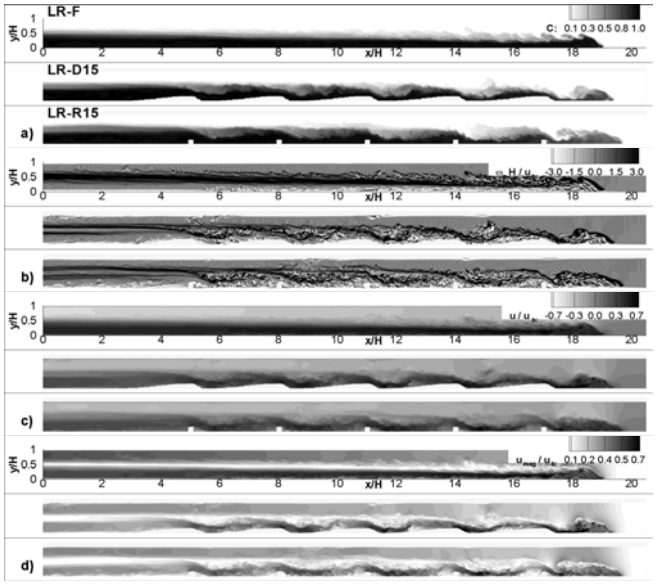

Figure 3 Visualization of the structure of the tail in the simulations with a flat bed and with obstacles of height D=0.15H at times when the front is situated close to x/H=18.5. a) concentration, C; b) out-of-plane vorticity, $\omega_z H / u_b$; c) streamwise velocity, u/u_b, d) velocity magnitude, u_{mag}/u_b

The formation of the backward propagating hydraulic jump amplifies the strength of the upstream part of the shear layer associated with the jet-like flow. As the hydraulic jump propagates, the shear layer extends further upstream and becomes more horizontal. The shear later separates the layer of mixed fluid carried behind the jump with the ambient fluid above it. As the hydraulic jump reaches the obstacle situated behind the one where it originated, and propagates over this obstacle, the shear layer continues to expand upstream. At those locations two shear layers containing vorticity of the same sign can be observed. As time passes, these shear layers merge and the interface with the top layer of ambient fluid becomes closer to horizontal. Thus, the variable height layer containing low-velocity mixed fluid is a result of the interaction of the backward propagating hydraulic jumps with the obstacle situated upstream from the one the jump originated and the jet-like flow over the upstream obstacles. The process of formation and temporal evolution of the shear layer are very similar in the case of dunes and ribs of height D=0.15H.

In the case ribs are present at the bed; a strong shear layer of vorticity of opposite sign to the one in the shear layer forming on the outer side of the jet-like flow is also present. On the other hand, in the case of dunes, a near-bed region of small velocity magnitude is present at about the middle of the leeside of the dune (e.g., around x/H=10, x/H=13 and x/H=16 in Fig. 3d). It is due to the fact that the core of high-velocity fluid within the jet-like flow is slightly diverted away from the dune surface. The flow does not separate.

5 2D MEAN FLOW AND TURBULENCE STRUCTURE IN BETWEEN TWO OBSTACLES SITUATED FAR FROM THE FRONT

In this section, the mean flow and turbulence structure in a region situated away from the head of the gravity current is analyzed after the flow reaches the quasi-steady regime in that region. The direct comparison of the distributions of the relevant variables predicted by the simulations with obstacles of height D=0.15H allows understanding in a quantitative way the effect of the shape of the obstacle on the flow and turbulence structure in the region where the quasi-steady regime is reached. These distributions allow an understanding of what are the similarities and differences in the flow and turbulence structure between the case of a stratified flow over a surface containing large-scale roughness and the widely studied case of a constant density flow propagating over the same large-scale roughness elements.

The non-dimensional distributions of the mean (spanwise and time-averaged) concentration, C, mean velocity magnitude, u_{mag}, mean out-of-plane vorticity, ω_z, and turbulent kinetic energy, k, are compared in Figs. 4 and 5 for the two simulations. The comparison is done in the region situated around the second obstacle. The length of this region is equal to the distance between the obstacles (λ=3H). In Figs. 4 and 5 the streamwise coordinate has the origin (x/λ=0) at the center of the rib or at the crest of the dune.

The mean concentration contours in Figs. 4a and 5a allow comparing the shape of the interface with the ambient (lighter) fluid in the simulations with ribs and dunes. In the discussion below the interface is defined as the position of the iso-concentration contour C=0.1. In both simulations the interface is situated at y/H~0.57 at x/λ=-0.33. In the case dunes are present at the bed, the elevation of the interface decreases fairly linearly until the crest (x/λ=0). The decrease continues until close to the location of the trough (x/λ~0.1) where y/H~0.52. Then, the elevation starts increasing. The maximum value (y/H~0.6) is reached at x/λ~0.5. The relative positions of the maximum and minimum of the interface elevation are in very good agreement with those measured by Mierlo and de Ruiter (1988) for a constant density channel flow over an array of identical dunes (channel Reynolds number was close to 20,000) and with the RANS predictions of the same flow by Yoon and Patel (1996). In their experiments the mean depth of the open channel flow was close to 0.6H which is close to the average position of the interface in the present gravity current simulations. The maximum relative difference in the interface position was $\Delta y_{max}/H$~0.01. As expected, this value is much smaller than the one recorded for the gravity current case ($\Delta y_{max}/H$=0.08) for which the relative density difference between the two fluids on the two sides of the interface, and thus the reduced gravity, is much smaller.

In the case ribs are present at the channel bottom, the interface elevation is close to constant (y/H~0.57) between x/λ=-0.33 and x/λ=-0.05. This region of constant elevation is followed by a region in which there is a sharp decay of the interface elevation ($-0.05<x/\lambda<0.13$). The minimum elevation is y/H~0.5. The flow over the rib resembles the channel flow over a weir. Between x/λ=0.13 and x/λ=0.6 the interface elevation increases monotonically before reaching a plateau value around y/H=0.57. Though experimental data are not available for the case of a constant density flow over an array of ribs of identical size and spacing to the present gravity current simulation to compare the variation of the free surface elevation, one can suspect the constant density flow case will show a similar trend in terms of the positions of the regions where the free surface elevation is increasing or decreasing.

Though for both types of roughness elements, a layer of high concentration fluid (C>0.8) is present in the bottom part of the domain, as shown in Figs. 4a and 5a, the height of this layer in the LR-D15 and LR-R15 simulations is different in several regions situated at an equal distance from x/λ=0. The comparison below starts at x/λ=-0.33 where the height of this layer is close in the two simulations (0.26H for dunes vs. 0.27H for ribs).

In case LR-D15 the height of the layer of high concentration fluid monotonically decreases as the crest is approached and then remains approximately constant (~0.15H) over the leeside of the dune and the trough region. Past x/λ=0.33 the thickness of this layer starts increasing again. It reaches a value close to 0.26H at x/λ=0.67. Thus, the maximum variation in the height of the layer of heavier fluid is only 0.11H. In contrast to this, the layer of mixed, lower concentration, fluid ($0.05<C<0.3$), in between the layer of heavier fluid and the layer of ambient fluid propagating in opposite direction, is subject to much larger height variations in the same region ($-0.33<x/\lambda<0.67$).

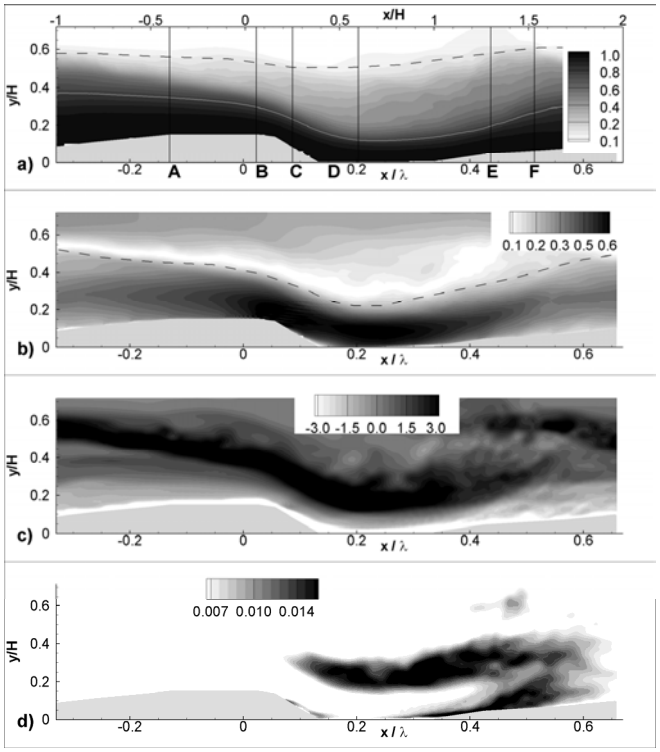

Figure 4 Mean flow and turbulence structure of the flow in the tail region after the quasi-steady regime is reached (LR-D15 simulation). a) concentration, C; b) velocity magnitude u_{mag}/U; c) mean out-of-plane vorticity, $\omega_z(H/U)$; d) turbulence kinetic energy, k/U^2. The mean variables were averaged in the spanwsie direction and in time, after the quasi-steady state was reached. The comparison is done in the region situated around the second obstacle in the series.

The presence of ribs with a blunt upstream face induces a gradual increase of the height of the layer of heavier fluid as the rib is approached. The height increases from 0.27H to 0.35H just upstream of the rib. The height of this layer over the rib is about 0.2H. Past the rib the height decreases sharply up to $x/\lambda=0.2$, where it reaches a value of 0.13H. The height of the layer of heavier fluid in this region is very close to the one in the simulation with dunes in the same region. Also, similar to the simulation with dunes, the height of the layer remains approximately constant for a certain distance (until $x/\lambda=0.45$ compared to $x/\lambda=0.33$ for dunes), after which it starts increasing again. Thus, most of the differences between the height of this layer in the LR-D15 and LR-R15 simulations occur in the region $-0.25<x/\lambda<0.2$. The differences will be much smaller if the height of this layer is defined such that it contains only heavier fluid that is convected in the streamwise direction. In other words, the height of the heavier fluid part of the recirculation regions forming upstream and downstream of the rib is not counted.

Indeed this is clearly seen from the comparison of the streamwise variation of the height of the layer of high velocity magnitude ($u_{mag}>0.2u_b$) in the simulations with dunes (Fig. 4b) and ribs (Fig. 5b). In both simulations, the top side of this layer is situated slightly above the upper interface of the layer of heavier fluid (C>0.8) over the whole length of the domain. The streamwise variation of the two interfaces is similar. In the case ribs are present at the channel bottom the height of this layer is approximately constant over the whole length of the domain, including the regions situated upstream and downstream of the rib. The average height of this layer of high velocity fluid propagating over the bed surface is about 0.3H.

In the case of dunes, the height of the layer of high velocity fluid varies between 0.5H at $x/\lambda=-0.33$ and 0.3H close to the crest and in the trough region. The top interfaces of the layers of high velocity fluid and of high concentration fluid are roughly parallel, with the interface of the layer of high velocity fluid situated slightly above the interface of the layer of high concentration fluid.

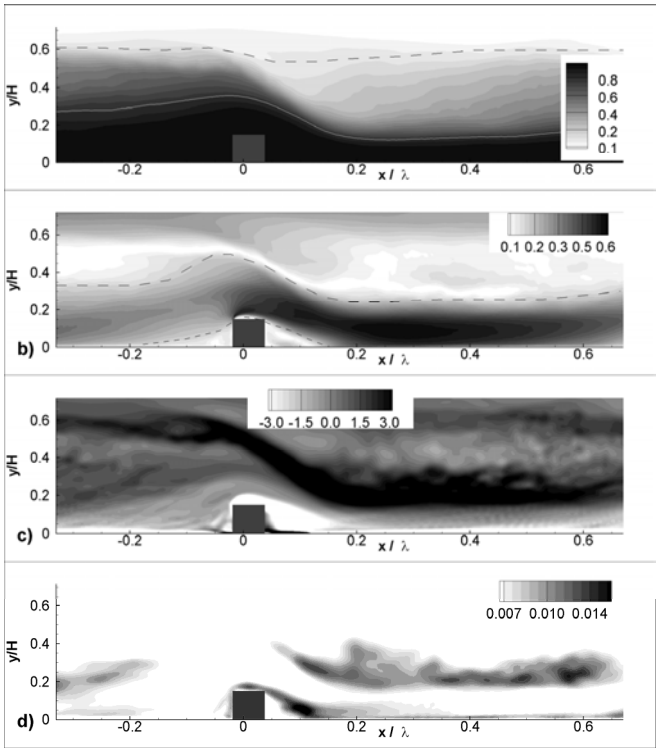

Figure 5 Mean flow and turbulence structure of the flow in the tail region after the quasi-steady regime is reached (LR-R15 simulation). a) concentration, C; b) velocity magnitude u_{mag}/U; c) mean out-of-plane vorticity, $\omega_z(H/U)$; d) turbulence kinetic energy, k/U^2. The mean variables were averaged in the spanwsie direction and in time, after the quasi-steady state was reached. The comparison is done in the region situated around the second obstacle in the series. The dashed and solid lines in frame a) correspond to the top of the layer of heavy fluid (C=0.8) and bottom of the layer of ambient fluid (C=0.1), respectively. The dashed line in frame b) corresponds to the top of the layer of high velocity magnitude.

In both simulations the region situated downstream of the top of the roughness element, where the jet-like flow is forming, contains mostly high concentration fluid (C>0.8). Thus, in both simulations the role of the layer of high velocity fluid is to advect mostly high concentration fluid over the

deformed bed surface. Observe also that the core of very large velocity magnitude ($u_{mag}>0.2u_b$) associated with the formation of the jet-like flow, as the heavier fluid is convected past the top of the roughness element, extends further downstream in the simulation with ribs. In other words, the penetration distance in the streamwise direction is larger in the case ribs are present at the channel bottom. This is also the reason the height of the layer of high velocity and high concentration fluid remains approximately constant for a longer distance downstream of $x/\lambda=0$ in the case ribs are present at the channel bottom.

The distribution of the out-of-plane vorticity ω_z in Figs. 4c and 5c show the presence of a strong shear layer of positive vorticity that covers thewhole length of the domain. As already discussed, this shear layer starts forming downstream of the crest/top of the roughness element on the outer boundary of the jet-like flow. Consistent with the different penetration length of the core of large streamwise velocity magnitude in Figs. 4b and 5b, the streamwise decay of vorticity in the shear layer is significantly sharper in the case dunes are present at the channel bottom (e.g., the tongue of high vorticity extends up to $x=0.5\lambda$ in the simulation with dunes and up to $x=0.67\lambda$ in the simulation with ribs). In the region with $0<x/\lambda<0.67$ the shape of the shear layer follows the one of the top interface of the layers of high velocity fluid and high concentration fluid. However, this is not the case in the regions situated at $-0.33<x/\lambda<0.0$ in Figs. 4b and 5b. Though a weak shear layer is still observed in both cases in the vicinity of the top interface of the layer of high concentration fluid (the vorticity is quite diffused in the simulation with ribs and much more concentrated in the simulation with dunes), the main region of high positive vorticity is situated at higher elevations. As already discussed, this region of high positive vorticity forms gradually in time as the shear layer forming on the outer side of the jet-like flow penetrates more and more in the upstream direction until it reaches equilibrium.

The distributions of ω_z in Figs. 4c and 5c correspond to this equilibrium regime. The upstream extension of the shear layer is a result of the interaction of the current of lighter fluid with the region containing mixed fluid and with the downstream part of the shear layer forming on the outer side of the jet like flow. At equilibrium, this tongue of positive vorticity can be observed starting at $x/\lambda=-0.33$. In both simulations it extends upstream for another 0.33λ. The tongue of vorticity around $y/H=0.6$ present between $x=0.33\lambda$ and $x=0.67\lambda$ correspond to this segment of the shear layer forming over the next roughness element. Thus, the shear layer extends up to -0.67λ for the roughness elements analyzed in Figures 4.16c and 4.17c. While in both simulations the shear layers are close to horizontal and situated at an elevation of about 0.6H at their upstream part ($-0.67<x/\lambda<-0.33$ or equivalently $0.33<x/\lambda<0.67$ according to Figures 4.16c and 4.17c) some differences are observed for $-0.33<x/\lambda<0.0$. While in the LR-R15 simulation the shear layer is still horizontal, in the LR-D15 simulation the shear layer becomes inclined, with a close to constant slope, as it connects the horizontal upstream part of the shear layer with the part situated close to the crest of the dune. In this region the position of the shear layer follows that of the top interface of the layer of large velocity fluid rather than that of the layer of high concentration fluid. The overall strength of the part of the main shear layer situated upstream of the crest/top of the roughness element ($-0.67<x/\lambda<0.0$) is larger in the LR-D15 simulation.

The distribution of the turbulence kinetic energy (tke) in Fig. 4d shows that in the simulation in which dunes are present at the channel bottom two regions of high tke develop downstream of the crest of the dunes. The tke levels inside the shear layer forming in the near-bed region as a result of the jet-like flow being deflected slightly away from the bed starting at $x/\lambda\sim0.33$ are similar to those inside the shear layer on the outer side of the jet-like flow. The tke amplification on the leeside of the dune is comparatively very small, as the flow remains attached. This is a main difference with the case of a constant density flow over a dune where a recirculation region and a strong separated shear layer form downstream of the crest.

In the LR-R15 simulation; a similar region of high tke values is present inside the shear layer on the outer side of the jet-like flow (see Fig. 5d). The non-dimensional values of tke are about 30% smaller compared to the simulation in which dunes are present at the channel bottom and its streamwise extent is larger (0.66λ for the ribs case compared to 0.45λ for the dunes case), which is consistent with the relative position and size of the core of large velocity magnitude inside the jet-like flow in the two simulations. The second region of high tke values corresponds to the separated shear layer forming at the upstream top corner of the rib. The tke levels remain relatively high even after the separated shear layer attaches to the horizontal part of the channel bottom. The tke levels are comparable to those in the shear layer forming on the outer side of the jet-like flow.

6 SUMMARY AND CONCLUSIONS

The present study investigated the changes in the flow and turbulence structure in the tail region of a turbulent bottom-propagating Boussinesq gravity current propagating over an array of 2D dunes or square ribs placed at the channel bottom based only on results of 3D LES simulations (no experimental data were available). The focus was on cases in which the shape and height of the obstacles (large-scale roughness elements with a height of 0.15H) was such that a relatively long slumping phase was present.

The temporal variation of the total volumetric flux of heavier fluid at selected streamwise locations showed that a quasi-steady regime is reached in between two consecutive obstacles at sufficiently large times after the passage of the front and after the backward propagating hydraulic jump forming at the downstream obstacle passed the obstacle situated upstream of it. The mean flow and turbulence structure was then investigated in the region between two consecutive obstacles, after the quasi-steady regime was reached. The characteristics of the flow in the tail of the current are important because for GCs with a large volume of release, if the current propagates in the slumping phase over a large number of obstacles, most of the sediment will be entrained from the bed beneath the tail, rather than beneath the head and dissipative wake regions as is the case for a current propagating over a flat bed.

REFERENCES

Chang, K.S., Constantinescu, S. G., Park, S. 2006. "Analysis of the flow and mass transfer processes for the incompressible flow past an open cavity with a laminar and fully turbulent incoming boundary layer, J. Fluid Mech., 561, 113-145.

Chang, K.S., Constantinescu, G., and Park, S.O., 2007, "The purging of a neutrally buoyant or a dense miscible contaminant from a rectangular cavity. Part II: The case of an incoming fully turbulent overflow", ASCE Journal of Hydraulics Engineering, Vol. 133, Issue 4, 373-385.

Cantero, M.I., Balachandar, S., Garcia, M.H.. 2006. "Direct numerical simulations of planar and cylindrical density currents. Journal of Applied Mechanics, Vol. 73, Issue 6, 923-930.

Gonzalez-Juez, E., Meiburg, E., and Constantinescu, G.S., 2009a, "Gravity currents impinging on bottom mounted square cylinders: Flow fields and associated forces", Journal of Fluid Mechanics, Vol. 631, 65-102.

Gonzalez-Juez, E., Meiburg, E., and Constantinescu, G.S., 2009b, "The interaction of gravity current with a circular cylinder mounted above a wall: Effect of the gap size", Journal of Fluids and Structures, Vol. 25, 629-640.

Gonzalez-Juez, E., Meiburg, E., T. Tokyay and Constantinescu, G.S. 2010, "Gravity current flow past a circular cylinder: Forces and wall shear stresses", Journal of Fluid Mechanics, Vol. 649, 69-102.

Hartel, C., Meiburg, E, and Necker, F., 2000, "Analysis and direct numerical simulation of the flow at a gravity-current head. Part 1. Flow topology and front speed for slip and no-slip boundaries", Journal of Fluid Mechanics, Vol. 418, 189–212.

Hatcher, L., Hogg, A.J., Woods, A.W., 2000) "The effects of drag on turbulent gravity currents", Journal of Fluid Mechanics, Vol. 416, 297-314.

Huang, H., Imran, J., and Pirmez, C., (2005) "Numerical model of turbidity currents with a deforming bottom boundary", ASCE Journal of Hydraulic Engineering, Vol. 131(4), 283-293.

Mierlo, M.C. and de Ruiter, J.C., 1988. "Turbulence measurements over artificial dunes", Report Q789. Delft Hydraulics Laboratory, Delft, Netherlands.

Ooi, S.K., Constantinescu, S.G., and Weber, L. 2009, "Numerical simulations of lock exchange compositional gravity currents", Journal of Fluid Mechanics, Vol. 635, 361-388.

Ooi, S.K., Constantinescu, S.G., and Weber, L. 2007a, "A numerical study of intrusive compositional gravity currents", Physics of Fluids Vol.19.

Ooi, S.K., Constantinescu, S.G., and Weber, L. 2007b, "Two-dimensional large-eddy simulation of lock-exchange gravity current flows at high Grashof numbers", ASCE Journal of Hydraulic Engineering, Vol. 9, 1037–1047.

Shin, J., Dalziel, S., and Linden, P.F., 2004, "Gravity currents produced by lock exchange", Journal of Fluid Mechanics, Vol. 521, 1-34.

Tanino, Y., Nepf, H.M., and Kulis, P.S., 2005, "Gravity currents in aquatic canopies", Water Resources Research, Vol. 41.

Yoon, J.Y. and Patel, V.C., 1996, "Numerical model of turbulent flow over sand dune", ASCE Journal of Hydraulic Engineering, Vol. 1, 10-18.